EARTHQUAKE ENGINEERING AND STRUCTURAL DYNAMICS, VOL. 25, 653–669 (1996)

# LARGE AMPLITUDE LIQUID SLOSHING IN SEISMICALLY EXCITED TANKS

WEI CHEN*
*Department of Civil and Environmental Engineering, University of California, Irvine, CA 92717, U.S.A.*

MEDHAT A. HAROUN†
*Department of Civil and Environmental Engineering, University of California, Irvine, CA 92717, U.S.A.*

AND

FENG LIU‡
*Department of Mechanical and Aerospace Engineering, University of California, Irvine, CA 92717, U.S.A.*

## SUMMARY

An innovative method of analysis was developed to simulate the non-linear seismic finite-amplitude liquid sloshing in two-dimensional containers. In view of the irregular and time-varying liquid surface, the method employed a curvilinear mesh system to transform the non-linear sloshing problem from the physical domain with an irregular free-surface boundary into a computational domain in which rectangular grids can be analysed by the finite difference method. Non-linearities associated with both the unknown location of the free surface and the high-order differential terms were considered. The Crank–Nicolson time marching scheme was employed and the resulting finite difference algorithm is unconditionally stable and very lightly damped with respect to the temporal co-ordinate. In order to minimize numerical instability caused by the computational dispersion in spatially discretized surface wave, a second-order dissipation term was added to the system to filter out the spurious high-frequency waves. Sloshing effects and structural response were measured in terms of sloshing amplitude, base shear and overturning moment generated by the hydrodynamic pressure of the liquid exerted on the container walls. Simulation results of liquid sloshing induced by earthquake and harmonic base excitations were compared with those of the linear wave theory and the limitations of the latter in assessing the response of seismically excited liquids were addressed.

KEY WORDS: liquid sloshing; nonlinear large-amplitude waves; hydrodynamic pressure; seismic response; numerical stability and dissipation; physical and computational domains

## INTRODUCTION

Seismic safety of ground-based and elevated liquid-filled containers is of great concern because of the potential economic loss that might be incurred due to structural failure of the liquid container as well as the potential environmental impact the spilling of the contained liquid might have to the surrounding area. The hazardous effect of liquid sloshing and the extensive damage sustained by liquid-filled tanks were evident in past seismic events such as the 1964 Alaska, the 1964 Niigata, the 1968 Tokachi-Oki, the 1979 Imperial Valley, the 1983 Coalinga, and more recently, the 1989 Loma Prieta, the 1992 Landers and the 1994 Northridge earthquakes.

Efforts have been undertaken, through both analytical[1–7] and experimental[8–11] works, to understand the complex behaviour of liquid-filled tanks during seismic events and to mitigate the hazardous effects of

*Postdoctoral Researcher, formerly graduate student
†Professor and Chair
‡Assistant Professor

CCC 0098–8847/96/070653–17


*Received 6 January 1994*
*Revised 28 February 1995*

seismically induced liquid sloshing on container structures. The outcome of an overall analysis of a seismically excited liquid-structure system, and the accuracy of the analysis, directly depend on how the liquid model involved resembles its physical properties and its accuracy in determining the liquid response under a given excitation. A foremost task in evaluating the seismic safety of a liquid container is to evaluate the hydrodynamic forces of the sloshing liquid exerted on the interfacing structure. In the case of flexible tanks, the effects of the liquid sloshing and the hydrodynamic impact on the structural response also need to be considered. Traditionally, the small-amplitude wave theory has been used exclusively in evaluating the seismic performance of liquid-filled containers. A linear sloshing model proposed by Housner[4] has been widely used and adopted in current ground-based tank standards such as the API 650[12] and the AWWA D100[13] because of its simplicity. On the other hand, the non-linear wave approach has not been attempted in predicting the *seismic* response of tank structures because of its mathematical difficulties in determining the elevation of the unknown moving free-surface and in evaluating the geometrically non-linear boundary conditions on the liquid surface. The use of the linear wave theory has restricted in many ways the true behaviour of liquid sloshing. These restrictions may lead to underestimation of the structural response of the container. For example, the underestimation of the sloshing height leads to an unsafe freeboard design in the container which already caused numerous damages in the roof-wall connection during past earthquakes.

Attempts have been made to understand analytically the behaviour of non-linearly sloshing liquids under base excitations by perturbation methods[8,14] and by the finite element and boundary element simulations[11,15–17] on digital computers. However, these models have yet to be directly applied to problems involving liquid containers subjected to seismic base excitations for an extended period of time (usually between 20 and 60 s). The seismic ground motion records usually have high level of excitation ( $> 0.2$ g) and the motion is non-harmonic. Numerical instabilities may occur at different stages of a sloshing simulation, depending on the algorithm used in discretizing the wave equation on the free surface, which range from excessive computational errors to the conditional stability of the algorithm involved. The latter leads to the restriction on grid resolution and the reduction in time steps. In this study, the finite difference approach was adopted because of the lower level of computational intensity compared to the finite-element-based methods, especially when large-scale grids are required. An advantage of the current model is its treatment of the unknown and moving surface of the liquid domain by introducing curvilinear co-ordinates so that the physical liquid domain with the irregular boundary is transformed into a computational domain consisting of straight grid lines on which the sloshing problem is discretized. The tank flexibility and irregularity can be taken into consideration under the framework of the current approach. The wave amplitude, the hydrodynamic pressure distribution, the base shear and the overturning moment exerted on the liquid container were obtained. These results were compared with the predictions by the linear wave theory and the adequacy and limitations of the latter were assessed.

## SLOSHING PROBLEM

The liquid considered in this study is assumed to be ideal, i.e. inviscid, incompressible and irrotational. The liquid container is represented by a two-dimensional rectangular domain with rigid walls as shown in Figure 1, where the undisturbed liquid depth is $H$ and the base width is $2a$. In order to simplify the problem, the flexibility of the walls was not considered. The equations governing the liquid motion under arbitrary horizontal base excitation can be expressed in terms of the relative Cartesian co-ordinates $(x, y)$ and the relative velocity potential $\phi$ as follows.[18]

$$\nabla^2\phi = 0 \qquad \text{in } \Omega \tag{1}$$

$$\frac{\partial\phi}{\partial x} = 0 \qquad \text{at } x = \pm a \tag{2}$$

$$\frac{\partial\phi}{\partial y} = 0 \qquad \text{at } y = -H \tag{3}$$

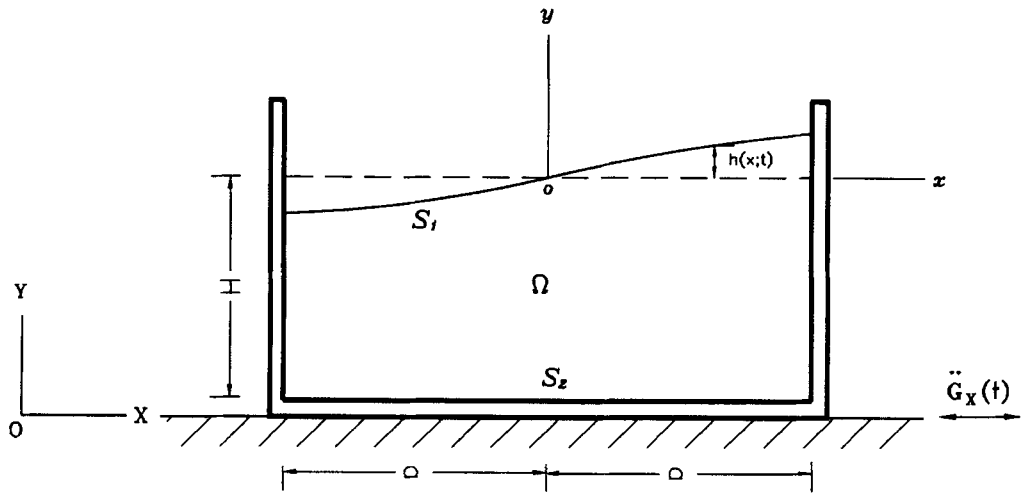


Figure 1. Liquid sloshing in two-dimensional domain

$$\frac{\partial h}{\partial t} + \frac{\partial \phi}{\partial x}\frac{\partial h}{\partial x} - \frac{\partial \phi}{\partial y} = 0 \qquad \text{at } y = h \tag{4}$$

$$\frac{\partial \phi}{\partial t} + \frac{1}{2}(\nabla\phi)^2 + x\ddot{G}_X + gh = 0 \qquad \text{at } y = h \tag{5}$$

where $h$ is the elevation of the perturbed liquid surface measured from its mean level, $g$ is the gravitational acceleration, $\Omega$ is the deformed liquid domain and $\ddot{G}_X$ is the horizontal ground acceleration. The relation between the velocity potential $\phi$ and the relative velocity of the liquid $\mathbf{u}$ is

$$\mathbf{u} = \nabla\phi \tag{6}$$

The boundary/initial value problem defined in equations (1)–(5) is a Laplace problem with non-linear boundary conditions imposed on the free surface. The non-linearity manifests itself in two ways: the elevation of the moving free surface is not known *a priori* at any given time instant and the boundary conditions on the free surface, equations (4) and (5), contain second-order differential terms. The initially quiescent liquid gives rise to the initial conditions

$$\phi(x, y; 0) = 0 \tag{7}$$

$$h(x; 0) = 0 \tag{8}$$

## LIQUID PRESSURE AND GENERALIZED FORCES

The hydrodynamic pressure of the seismically excited liquid can be obtained from Bernoulli's equation[19] as

$$\frac{p(x, y; t)}{\rho} = -\frac{\partial \phi}{\partial t} - \frac{1}{2}(\nabla\phi)^2 - x\ddot{G}_X - gy \tag{9}$$

where $p(x, y; t)$ is the hydrodynamic pressure and $\rho$ is the mass density of liquid.

The total shear force at the base of the tank $Q$ at a given time $t_0$ can be obtained by integrating the pressure along the two side walls

$$Q(t_0) = \int_{-H}^{h(-a,t_0)} p(-a, y; t_0)\,dy - \int_{-H}^{h(a,t_0)} p(a, y; t_0)\,dy \tag{10}$$

and similarly, the overturning moment can be evaluated from

$$M(t_0) = -\int_{-H}^{h(-a,t_0)} y \cdot p(-a, y; t_0)\,dy + \int_{-H}^{h(a,t_0)} y \cdot p(a, y; t_0)\,dy + \int_{-a}^{a} x \cdot p(x, -H; t_0)\,dx \tag{11}$$

Note that the integrations on the side boundaries are carried out between $(-H)$ and the true liquid surface $h$. The integrals in equations (10) and (11) can be evaluated numerically once the discretized values of equation (9) are obtained.

## LINEAR THEORY

The forced liquid sloshing problem, described by equations (1)–(5), can be linearized by ignoring the higher-order differential terms in the boundary conditions on the free surface and by imposing these conditions on the mean surface, $y = 0$, rather than on the moving surface, $y = h$. The closed-form solution of $\phi$ takes the following form:

$$\phi(x, y; t) = \sum_{n=1}^{\infty} \dot{C}_n(t) \sin(\alpha_n x) \cosh(\alpha_n (y + H)) \tag{12}$$

where $\dot{C}_n(t)$ denotes derivative of $C_n$ with respect to time and can be determined from the following ordinary differential equation:

$$\ddot{C}_n + 2\zeta_n \omega_n \dot{C}_n + \omega_n^2 C_n = -\frac{(-1)^{n+1} 2}{\alpha_n^2 a \cosh(\alpha_n H)} \ddot{G} \quad (n = 1, 2, \ldots) \tag{13}$$

In equations (12) and (13), $\zeta_n$ is the added damping ratio to simulate liquid viscosity, and $\alpha_n$ and $\omega_n$ are the $n$th wave number and natural frequency, respectively, given by

$$\alpha_n = \frac{(2n-1)\pi}{2a} \tag{14}$$

$$\omega_n^2 = \alpha_n g \tanh(\alpha_n H) \tag{15}$$

Equation (13) can be integrated numerically when the base motion is not periodic.[18] A simplified computation of the maximum sloshing amplitude can be obtained by separating the impulsive and convective parts in the velocity potential function and considering the latter only

$$|h_{\max}| = \frac{8a}{\pi^2 g} \sum_{n=1}^{\infty} \frac{S_{an}}{(2n-1)^2} \tag{16}$$

where $a$ is half-width of the tank base and $S_{an}$ is the spectral acceleration corresponding to the $n$th liquid frequency. Note that in obtaining equation (16), a zero damping ratio is assumed. Code stipulation on the maximum sloshing amplitude is based on equation (16) by ignoring higher modes:

$$|h_{\max}| \doteq 0{\cdot}81 \frac{aS_{a1}}{g} \tag{17}$$

A numerical example is now given in which the values of the maximum sloshing amplitude at $x = -a$ of a liquid having $a = 4{\cdot}572$ m (15 ft) and $H/a = 0{\cdot}5$ are computed. The liquid is excited at its base by four earthquake ground motions: the 1940 El Centro earthquake, both EW and NS components, the 1989 Foster City record and the 1985 Mexico City SCT1 record. For each of the ground motions, two cases are

Table I. Linear sloshing amplitude

| Earthquake records | 10 mode (cm) $\zeta = 0{\cdot}5$ per cent | 1 mode (cm) $\zeta = 0$ per cent | $\Delta$ per cent |
|---|---|---|---|
| El Centro (EW) | 42·88 (16·88″) | 44·45 (17·50″) | 3·7 |
| El Centro (NS) | 27·03 (10·64″) | 22·96 (9·04″) | 15·1 |
| Foster City | 38·46 (15·14″) | 35·61 (14·02″) | 7·4 |
| Mexico City SCT1 | 133·58 (52·59″) | 59·51 (23·43″) | 55·4 |

considered. In the first case, the sloshing is computed by the analytical procedure which includes 10 modes at a modal damping ratio $\zeta_n = 0{\cdot}5$ per cent; and in the second case, the response-spectrum based single-mode formula with 0 per cent damping is used. The results of the computation are listed in Table I, where the deviation of the peak values of the spectrum approach from the modal analysis results is also shown. It is seen that, with 0·5 per cent damping in the 10-mode cases, higher modes were mostly damped out except in the Mexico City case, in which the response of the higher modes plays a more significant role.

## CO-ORDINATE TRANSFORMATION

The liquid domain considered in this study has a moving free surface which makes it non-rectangular in shape. A curvilinear co-ordinate system is introduced to transform the sloshing problem from the physical domain $\Omega$ into a rectangular computational domain $\Omega'$, as shown in Figure 2. The sloshing problem was originally formulated in the physical domain and was transformed to and solved in the computational domain. A co-ordinate transformation is employed to map the Cartesian co-ordinates into the curvilinear ones, and *vice versa*, and the relation between the two co-ordinate systems is shown schematically in Figure 2. A necessary feature of the transformation is that the mapping is one to one. It is desirable, however, that the grid lines are boundary conforming. By transforming the sloshing problem into the computational domain, rectangular grids can be obtained for the finite difference discretization. The obvious advantage of introducing a curvilinear grid system is balanced by the fact that the transformed equations in the computational domain become much more complicated and lengthy. Detailed discussions on the transformation relations and the differential operators in curvilinear co-ordinates can be found in Reference 20.

Special attention was given to the time derivative terms in equations (4) and (5). It was noted that the grids in the computational domain are fixed whereas the grids in the physical domain move with time. In

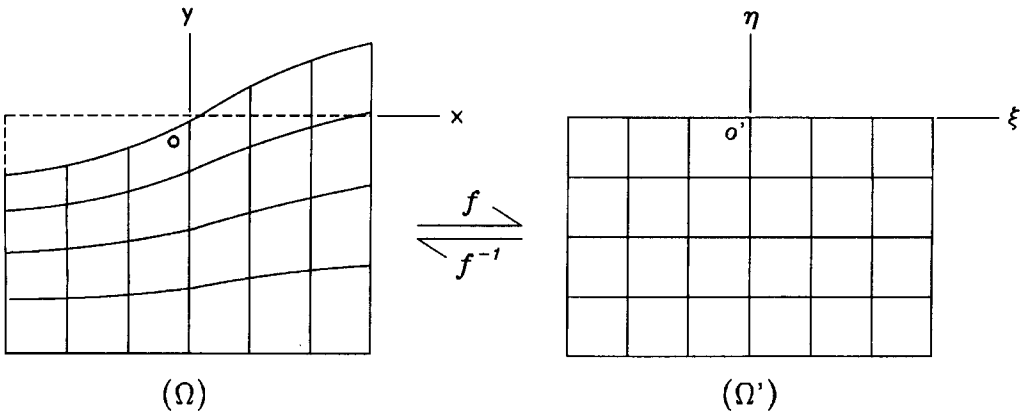


Figure 2. The physical and computational domains

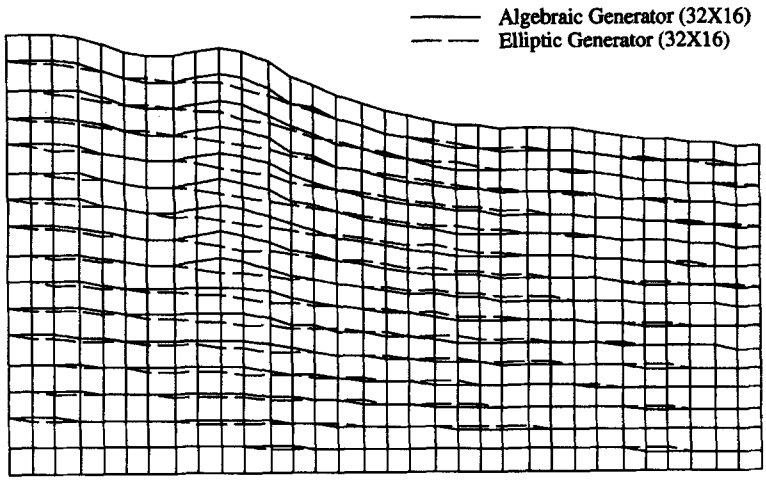


Figure 3. Curvilinear grids at $t = 13{\cdot}88$ s for liquid sloshing subjected to Foster City record

transforming the time derivative terms from the physical domain into the computational domain, there exists an additional convective term due to the moving physical grids. Hence, one has

$$\frac{\partial}{\partial t} f(\mathbf{r}; t) = \frac{\partial}{\partial t} f(\xi; t) - \nabla f(\xi; t) \cdot \frac{\mathrm{d}\mathbf{r}}{\mathrm{d}t} \tag{18}$$

where $f$ is an arbitrary differentiable scalar function, $\mathbf{r}$ and $\xi$ are the position vectors of the grid points in the physical and computational domains, respectively. An example of the numerical grids generated by an algebraic and elliptic PDE system is illustrated in Figure 3.

## SPATIAL FINITE DIFFERENCE

In discretizing equations (1)–(5), central finite differences are used for the approximations of the differential terms discretized at nodal points inside the computational domain $\Omega'$ and for derivatives at nodes on any of the four boundaries (excluding the four corner nodes) with differencing orientation along the respective boundary line. For a derivative term on any given boundary node with differencing orientation perpendicular to the boundary line, three-point forward or backward finite difference is used for approximation, depending on the orientation of the boundary concerned. The merit of this algorithm is that the overall accuracy of the spatial discretization is of the second order. The drawback is that, comparing to the spatial discretizations in which first-order forward or backward difference is employed on the boundaries, the symmetries of the discretized Laplace problem with respect to the $\xi$- and $\eta$-axes are destroyed and, consequently, numerical leakage of the liquid mass may occur on the boundaries. However, it will be seen later that this non-conservative property of the liquid mass has insignificant effect on the numerical solution of the sloshing problem.

At each of the four corner nodes of the liquid domain, the boundary conditions from each of the boundaries connecting that node are supposed to be satisfied simultaneously. However, due to the redundancy of the discretized equations at corner nodes, only *one* boundary condition can be satisfied for the two lower corner points and *two* conditions for the two top corners. Since the conditions on the two side boundaries ($\xi = 1$ and $\xi = \mathrm{IMAX}$) govern the reflection of the surface gravity waves and determine how the base motion input is felt by the liquid, they are made to be satisfied at all of the corner points. On the free surface, the kinematic condition, equation (4), is enforced at the two top corner nodes since it represents more of a boundary property at these two points.

## TIME MARCHING SCHEME

The Crank–Nicolson time marching scheme is employed for the equations which explicitly involve time, equations (4) and (5). It is an implicit time-centred marching scheme with a second-order accuracy. For a differential equation of the form

$$\frac{\partial f}{\partial t} = G(x, f, f_x, f_{xx}, \dots) \tag{19}$$

the Crank–Nicolson scheme gives rise to

$$\frac{f_i^{n+1} - f_i^n}{\Delta t} = G(x_i, f_i^{n+1/2}, (f_x)_i^{n+1/2}, (f_{xx})_i^{n+1/2}, \dots) = G_i^{n+1/2} \tag{20}$$

where the superscript and subscript denote discretized temporal and spatial grid points, respectively. For instance, $f_i^{n+1/2}$, indicates that the function $f$ is evaluated at time $(n + \frac{1}{2})\Delta t$ and node $x = (\mathrm{i}\,\Delta x)$, respectively, where $\Delta t$ and $\Delta x$ are the temporal and spatial increments of discretization. The temporal reference point is centred at node $(n + \frac{1}{2})\Delta t$. Instead of evaluating the function value of $G_i$ at time $(n + \frac{1}{2})\Delta t$, the last term on the right-hand side of equation (20) is approximated by the average value of $G_i$ at the two neighbouring integer points

$$G_i^{n+1/2} = \frac{G_i^n + G_i^{n+1}}{2} \tag{21}$$

It is worth noting that, although equations (1)–(3) do not explicitly involve temporal coordinate $t$, these equations should be treated in the same fashion as in equation (21), thus making the whole discretized system consistent. Discussion on spatial and temporal discretization of PDE using finite difference schemes and algorithm stability can be found in a reference by Minkowycz *et al.*[21]

## NON-LINEAR TREATMENT

There are $2 \times (\mathrm{IMAX} - 1)$ non-linear equations on the top boundary of the liquid domain, where IMAX is the total number of grid points in the $\xi$-direction, and these non-linear equations are coupled with the rest of the discretized linear equations to form a system of $\mathrm{IMAX} \times (\mathrm{JMAX} + 1)$ equations. Instead of treating the whole system of equations as non-linear, linearization similar to that of the Newton–Raphson method is performed and the corresponding Jacobian elements are evaluated for the $2 \times (\mathrm{IMAX} - 1)$ non-linear equations only. The resulting equations are combined with the rest of the equations and iterated at each time step until convergence is reached. To this end, one has the following iteration scheme:

$$J({}^k\mathbf{z})^{k+1}\mathbf{z} = J({}^k\mathbf{z})^k\mathbf{z} - \mathbf{F}({}^k\mathbf{z}) \tag{22}$$

where ${}^k\mathbf{z}$ is the unknown vector from the previous iteration, $\mathbf{F} = (f_1, f_2, \dots, f_n)$ is a vector of $(n = 2(\mathrm{IMAX} - 1))$ differentiable non-linear functions and $J({}^k\mathbf{z})$ is the Jacobian matrix defined as follows:

$$J(\mathbf{z}) = \begin{bmatrix} \dfrac{\partial f_1(\mathbf{z})}{\partial z_1} & \dfrac{\partial f_1(\mathbf{z})}{\partial z_2} & \cdots & \dfrac{\partial f_1(\mathbf{z})}{\partial z_n} \\ \dfrac{\partial f_2(\mathbf{z})}{\partial z_1} & \dfrac{\partial f_2(\mathbf{z})}{\partial z_2} & \cdots & \dfrac{\partial f_2(\mathbf{z})}{\partial z_n} \\ \vdots & \vdots & & \vdots \\ \dfrac{\partial f_n(\mathbf{z})}{\partial z_1} & \dfrac{\partial f_n(\mathbf{z})}{\partial z_2} & \cdots & \dfrac{\partial f_n(\mathbf{z})}{\partial z_n} \end{bmatrix} \tag{23}$$

The iteration is considered converged when the norm of the difference of the unknown vectors from two successive iterations satisfies the condition

$$\| {}^{k+1}\mathbf{z} - {}^{k}\mathbf{z} \|_{\infty} \leqslant \varepsilon \tag{24}$$

where $\varepsilon$ is a prescribed tolerance of error.

## COMPUTATIONAL CONSIDERATION

The linear system resulting from the discretized sloshing problem is a banded sparse matrix. The vectorized LU solver on the CONVEX C240-1024 mini super computer at the University of California, Irvine, is used to solve the iterative linear system. A simulation was also run by using SOR method to solve the linear system. It was found that, for a mesh of size $32 \times 16$, LU library routine resulted in less CPU time consumption than that by the SOR method, which was partly due to the highly vectorized code. It is expected, however, the rate of the CPU increase of the LU routine will be much higher than that of the SOR method when the mesh size grows. Typically, a simulation with the mesh size mentioned above consumed about 45 min of CPU time on the CONVEX.

## NUMERICAL INSTABILITY AND ADDED DISSIPATION

For the finite difference schemes outlined above, a sloshing simulation was conducted for a liquid (water) with $2a = 1{\cdot}0$ m and $h = 0{\cdot}5$ m and excessive computational error was found to exist in the wave-propagating boundary condition, equation (4). The numerical case tested is the same as the one used in the shaking-table test and the finite element study of two-dimensional liquid sloshing by Okamoto[11] and Okamoto and Kawahara.[16] The base excitation was harmonic with a frequency $\bar{\omega} = 5{\cdot}311$ rad/s and a low-level amplitude $A_{\max} = 0{\cdot}93\,\bar{\omega}^2$ cm/s$^2$ (0·03 g). The numerical value for the convection term $(h_x\phi_x)$ became dominant for the given excitation and the simulation was broken down at $t = 11{\cdot}54$ s. In Figure 5, a sequence of the unstable surface-wave profiles are plotted at intervals $\Delta t = 0{\cdot}04$ s between $t = 10{\cdot}44$ s and $t = 11{\cdot}54$ s. A build-up of high-frequency waves is visible on the liquid free-surface (solid lines in Figure 5) as time progressed. The sloshing amplitude at $x = -a$ predicted by the current model using a $24 \times 20$ mesh and $\Delta t = 0{\cdot}01$ s is plotted against time by a dashed line in Figure 4 and the numerical divergence is indicated by a circle.

In order to stabilize the numerical solution, a second-order numerical dissipation term was introduced in the kinematic boundary condition, equation (4), which gives rise to

$$\frac{\partial h}{\partial t} + \phi_x \frac{\partial h}{\partial x} - \mu\left(\nu \frac{\partial^2 h}{\partial x^2}\right) - \phi_y = 0 \tag{25}$$

where $\mu$ is a constant whose value is between 0·0 and 1·0, and $\nu$ is a coefficient that is determined from the following expression:

$$\nu = \tfrac{1}{2}\Delta x |\phi_x| \tag{26}$$

When $\mu = 1{\cdot}0$, the resulting differencing scheme of $h_x$ in equation (25) is the so called *upwinding* scheme. The numerical instabilities and artificial damping are discussed in more detail in a separate paper[22] and computational dispersion in finite difference/finite element method was discussed by Pinder and Gary.[23] The introduction of the coefficient $\mu$ is to scale the amount of the numerical dissipation to a minimum level that is necessary to stabilize a numerical solution. The afore-mentioned sloshing simulation (dashed line in Figure 4) was repeated after adding 30 per cent of the dissipation ($\mu = 0{\cdot}30$) specified by equation (26). The simulation completed successfully at the designated 20 s mark. The resulting time history of sloshing amplitude is shown by the solid line in Figure 4, in which a linear finite difference solution without numerical dissipation is also shown, and the corresponding wave profiles are shown in Figure 5 by dashed lines. It is seen that, with

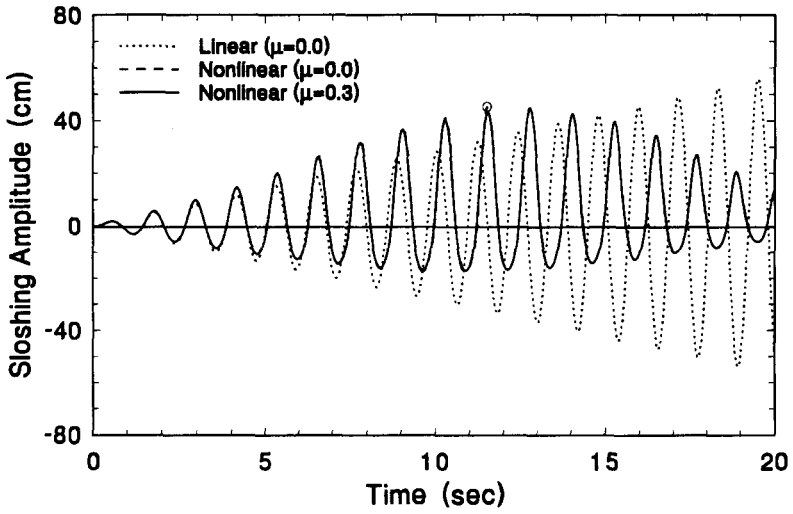


Figure 4. Sloshing amplitude at $x = -a$

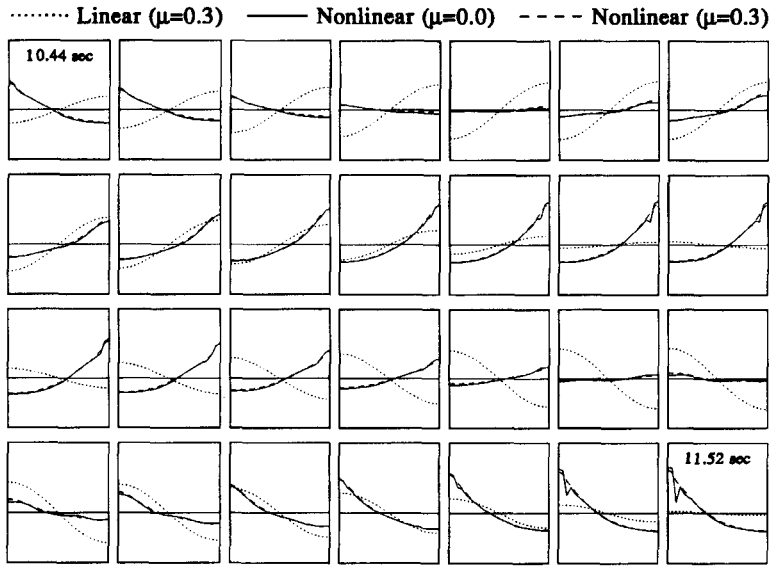


Figure 5. Profiles of surface wave at 0·04 s intervals

numerical dissipation added, the high-frequency wiggles represented by the solid lines in Figure 5 have disappeared. It is also observed that:

(1) The minimum value of $\mu$ required to achieve a stable numerical solution in Figure 4 is 0·27. The diffusion effect of the added numerical dissipation on the magnitude of sloshing amplitude is invisible in Figures 4 and 5 and, considering the fact that Figure 5 is plotted to scale, the decaying of the amplitude is insignificant for engineering applications. The sensitivity of the seismically induced sloshing response to the selection of $\mu$-value is addressed in a separate section of this paper.
(2) The non-linear sloshing amplitude, as observed in other studies, has an upward shifting about the time axis as shown in Figure 4, in which the growth of the positive amplitude is much faster than that of the negative amplitude. Generally, the more intense the sloshing, the more severe the upward skewing.

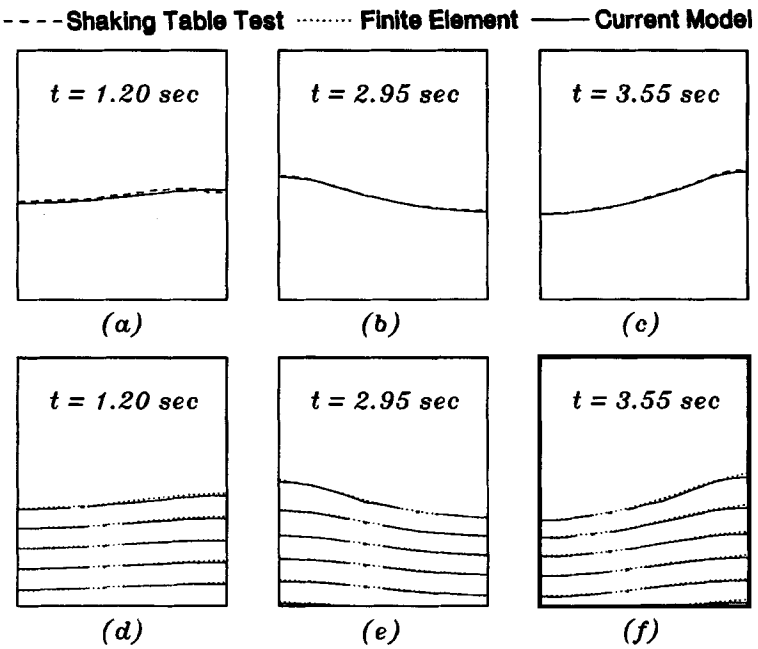


Figure 6. Comparison of present model with available results ((a)–(c): free surface elevation; (d)–(f): hydrodynamic pressure contour)

However, this inherent behaviour of the large-amplitude liquid sloshing should be differentiated from the gradual elevation or depletion of the sloshing amplitude due to mass imbalance, which is a numerical behaviour.

(3) The forcing frequency of the base motion in Figure 4 is fairly close to that of the fundamental natural frequency of the liquid ($\omega_1 = 5.317$ rad/s). The behaviours of the linear and non-linear resonant sloshing amplitude are strikingly different. Whereas the linear response resembles that of a resonant single degree-of-freedom undamped linear oscillator, the non-linear response exhibits an amplitude modulation behaviour (Figure 4) and a softening behaviour which is characterized by period elongation (Figures 4 and 5).

To verify the validity of the proposed sloshing model, numerical simulation results of the finite difference model were compared with the shaking-table test and finite element results of Okamoto[11] and Okamoto and Kawahara.[16] In Figure 6(a)–6(c) with the same data used, the free surface profiles of the sloshing liquid at $t = 1{\cdot}20$, $2{\cdot}95$ and $3{\cdot}55$ s are compared with the corresponding results of a shaking-table test of a thin rectangular tank.[11] The base excitation is sinusoidal with an amplitude of $0{\cdot}03g$, where $g$ is the gravitational acceleration. Hydrodynamic pressure contours are also plotted in Figure 6(d)–6(f), with solid lines representing the finite difference model and dotted lines representing the finite element model by Okamoto[11] and Okamoto and Kawahara.[16] It is seen that the simulation results from the proposed model match very well with those of the test and the finite element model.

## LIQUID MASS IMBALANCE

The unsymmetric three-point finite difference in the $\xi$-direction on the two opposing side boundaries and the added numerical dissipation are (both) possibly responsible for the mass imbalance of liquid, which is manifested by the gradual upward shifting of the sloshing amplitude with time as if the time-history curve rotates counter-clockwise (mass injection) or clockwise (mass depletion) about the axis origin. The level of mass accumulation for a liquid of dimensions $a = H = 4{\cdot}572$ m subjected to a harmonic base motion $\ddot{G}_X = (0{\cdot}1g)\cos(1{\cdot}17\omega_1 t)$, where $\omega_1$ is the fundamental natural circular frequency of the liquid, is illustrated in

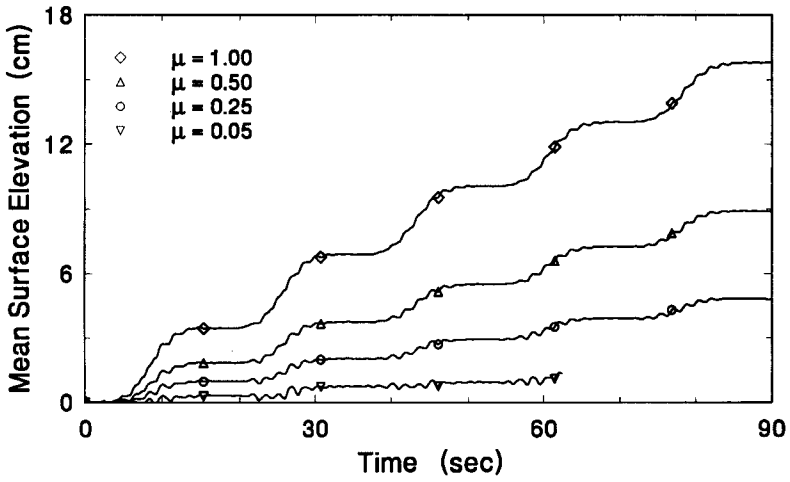


Figure 7. Effect of numerical dissipation on mass conservation

Figure 7 by the mean elevation of the free surface. The mean surface elevation is zero initially and should remain so if the liquid mass is to be conserved. For $\mu = 0{\cdot}25$, the average elevation of the mean-liquid-surface at $t = 90$ s is about 4·8 cm (1·9 in), which amounts to about 1 per cent of the total mass of the liquid. It also shows that, when $\mu = 0{\cdot}05$, the mass change is kept under 1·0 cm for the first 60 s of simulation, which indicates that the aforementioned unsymmetric spatial discretization scheme has a minimal effect in causing mass imbalance.

## SEISMIC RESPONSE OF LIQUID

Having confirmed the validity of the present method, simulations of large-amplitude sloshing were conducted for liquid subjected to four earthquake base excitations: the Coyote Lake Dam record (COMP N75E), the El Centro Imperial Valley record (COMP S90W), the Foster City record and the Mexico City SCT1 record (COMP N90W). Among these seismic records, the Mexico City SCT1 record is known for its long-period components with predominant period at about 2 s. This is important for liquid response because liquid in containers usually has a significantly longer fundamental natural period than most of the building structures. A liquid container with the base-width of 9·14 m (30 ft) and the height of 6·10 m (20 ft) is filled with water to a depth of 4·57 m (15 ft). The amount of numerical dissipation used in the numerical simulations are: $\mu = 0{\cdot}025$ for the Coyote Lake Dam record, the El Centro record (EW) and the Foster City record, and a higher level of $\mu = 0{\cdot}85$ for the Mexico City case because of the intense surface sloshing of the liquid generated by the predominantly long-period and steady-state-like base motion. The selection and the effects of the $\mu$-value are discussed in a separate section.

It was shown that large-amplitude sloshing produced a constant upward shifting of sloshing amplitude, which is of great interest in earthquake engineering application because of the damaging effects it produces in the upper part of the tank structure due to the pounding of the surface wave. Hence, the *positive* maximum sloshing amplitude was recorded rather than the global peak responses. In Table II, linear and non-linear positive sloshing amplitudes at $x = -a$ and $x = a$ and the percentage increase of the non-linear response over the linear response are listed. Among the four seismic records, the Mexico City SCT1 record generated pronounced amplitude response, both in terms of absolute peak values as well as the percentage increase of the non-linear peak amplitude over the linear one. It is seen that the linear wave theory is overly non-conservative in estimating sloshing amplitude in some cases, such as the peak sloshing amplitude at $x = a$ in the case of the Mexico City record because of the predominantly long-period components present in the seismic accelerogram. The time histories of liquid sloshing induced by the El Centro EW record and the Mexico City record are plotted in Figures 8 and 9, respectively, where linear peaks are marked by circles. It is

Table II. Comparison of linear and non-linear peak wave amplitude

| Earthquake record | Amplitude (+) at $x = -a$ | | | Amplitude (+) at $x = a$ | | |
|---|---|---|---|---|---|---|
| | Linear (cm) | Non-linear (cm) | Δ per cent | Linear (cm) | Non-linear (cm) | Δ per cent |
| C.L. Dam | 26·5 | 29·2 | 10·4 | 24·6 | 26·7 | 8·5 |
| El Centro | 50·6 | 65·0 | 28·4 | 56·6 | 69·6 | 22·9 |
| Foster City | 69·8 | 80·9 | 15·9 | 57·3 | 73·3 | 27·8 |
| Mexico City | 135·1 | 198·7 | 47·0 | 110·5 | 204·5 | 85·1 |

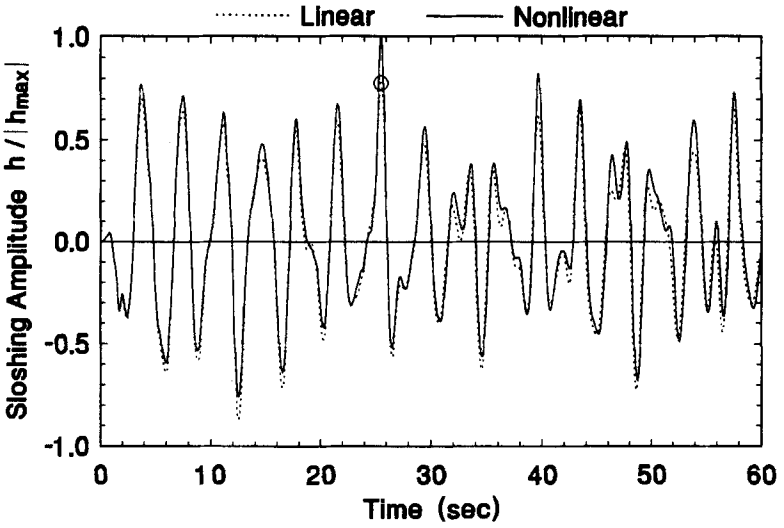


Figure 8. Linear and non-linear wave amplitude at $x = -a$ due to El Centro record

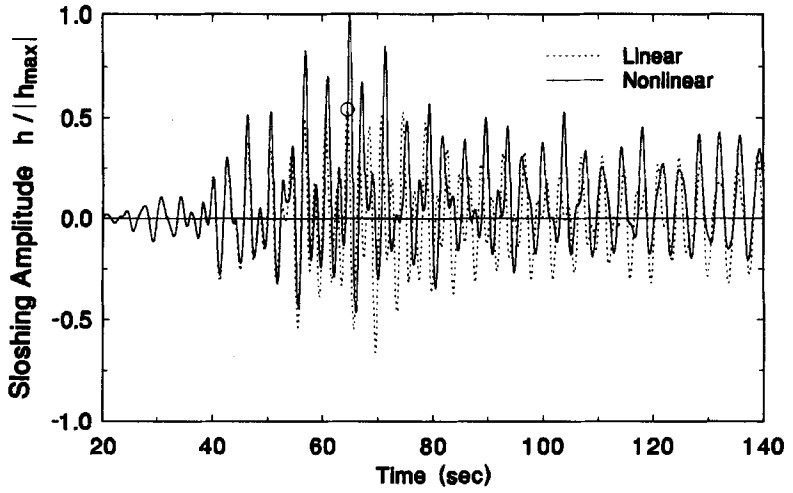


Figure 9. Linear and non-linear wave amplitude at $x = a$ due to Mexico City SCT1 record

Table III. Comparison of linear and non-linear peak base shear and overturning moment

| Earthquake record | Base shear $\|Q_{max}\|$ | | | Overturning moment $\|M_{max}\|$ | | |
|---|---|---|---|---|---|---|
| | Linear (kN) | Non-linear (kN) | Δ per cent | Linear (kN m) | Non-linear (kN m) | Δ per cent |
| C.L. Dam | 37·71 | 37·61 | − 0·3 | 140·03 | 139·84 | − 0·1 |
| El Centro | 51·40 | 52·32 | 1·8 | 193·21 | 195·52 | 1·2 |
| Foster City | 62·81 | 64·41 | 2·5 | 240·20 | 244·22 | 1·7 |
| Mexico City | 47·52 | 48·70 | 2·5 | 182·29 | 188·48 | 3·4 |

seen that the response to the Mexico City record exhibits pronounced nonlinear sloshing behaviour in terms of the upward shifting of amplitude and the period elongation, as compared to the sloshing amplitude of the El Centro EW record. It is also noted that, regardless of the base excitation input, sloshing amplitudes in Figures 8 and 9 oscillate predominantly at a frequency very close to the fundamental natural frequency of the liquid (0·28 Hz). However, in the case of Mexico City base excitation, there is a contribution of a sub-harmonic oscillation with a frequency close to that of the second-mode linear frequency of the liquid (0·506 Hz). Nevertheless, the non-linear sloshing behaviour did not predict a predominantly second-mode response as the linear theory would (Table I).

Linear and non-linear maxima of the base shear and overturning moment for the above cases are listed in Table III. In contrast to the sloshing amplitude, linear wave theory generally predicts the peak hydrodynamic forces reasonably well as compared to the non-linear theory. The time histories of the base shear and the overturning moment for the Mexico City records are plotted in Figures 10 and 11, respectively, where linear peaks are marked by circles. It should be stressed that, while the maximum response (global peak) is a critical measurement of the seismic effects of the liquid motion, repeated excursions of the secondary non-linear peaks over their linear counterparts in a given duration of time are equally detrimental for some cases because of the cumulative damage sustained by the container structure. Such a possibility is illustrated in Figure 12, where the overturning moment for a container with dimensions $a = 2H = 4{\cdot}57$ m (15 ft) and subjected to the Mexico City base excitation is shown. It is seen that the values of the global peaks of the linear and non-linear responses are fairly close ($|M^{max}_{linear}| = 93{\cdot}67$ kN m, $|M^{max}_{non\text{-}linear}| = 101{\cdot}04$ kN m). However, the non-linear response exceeds the linear counterpart by a consistent wide margin after approximately 60 s. This cumulative effect of non-linear forces should be taken into account in design.

## DISSIPATION EFFECTS

The criterion used for selecting the value of $\mu$ is based on a trial-and-error basis. Generally speaking, the selection of a value for $\mu$ should be proportional to the magnitude of the sloshing amplitude, the surface slope and the convection speed of the surface wave. The base excitation being considered is also an important factor in determining the value of $\mu$ — the more intense the base motion (high-level amplitude, frequency tuning with the liquid), the more the numerical solution is polluted by the computational dispersion error; hence, higher values of $\mu$ should be used.

The sensitivity of the sloshing amplitude induced by the Mexico City record and the El Centro record to the selection of the $\mu$-value is shown in Figures 13(a), 13(b) and 13(c), 13(d), respectively, where linear and non-linear free-surface heights were plotted for given values of $\mu$. The time instants in these plots represent the peak sloshing response at location $x = a$ on the free surface; the corresponding numerical values and the percentage change of sloshing amplitude are listed in Table IV. It is observed that, for the same amount of increase in $\mu$, the non-linear response decays faster than the linear prediction. In the case of non-linear sloshing due to the Mexico City record, $\mu = 0{\cdot}75$ is the lower bound for numerical stability (for a simulation of 200 s). However, the jagged free surface represented dispersion components of the solution and the

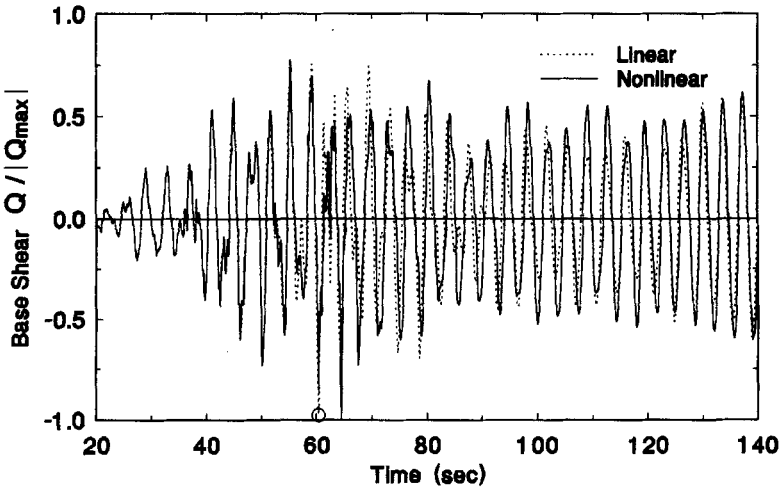


Figure 10. Linear and non-linear base shear due to Mexico City SCT1 record

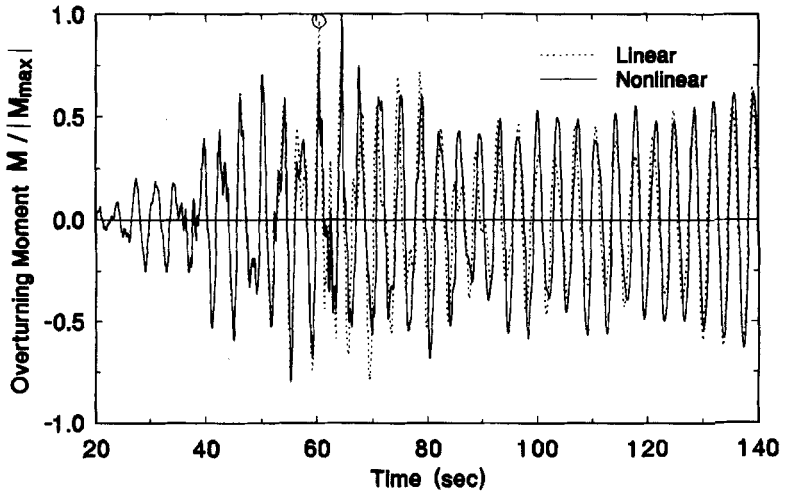


Figure 11. Linear and non-linear overturning moment due to Mexico City SCT1 record

corresponding prediction of the sloshing amplitude at $x = a$ was overshot (less than 4 per cent) as a result. It is argued that the decrease in peak sloshing amplitude and the general shape of the free surface are not severely altered by the introduction of the numerical damping and ought to be acceptable for engineering applications.

## CONCLUSIONS

An implicit finite difference approach is presented to simulate large-amplitude sloshing motion of liquid subjected to harmonic and earthquake base excitations. The PDE, defining the non-linear liquid sloshing problem which includes a free-moving surface, is transformed into a computational domain using a curvilinear co-ordinate system so that fixed and rectangular grids are obtained for spatial finite difference discretizations. The model is unconditionally stable due to its implicit nature and contains very little diffusion associated with the temporal discretization. A second-order numerical dissipation term is added to

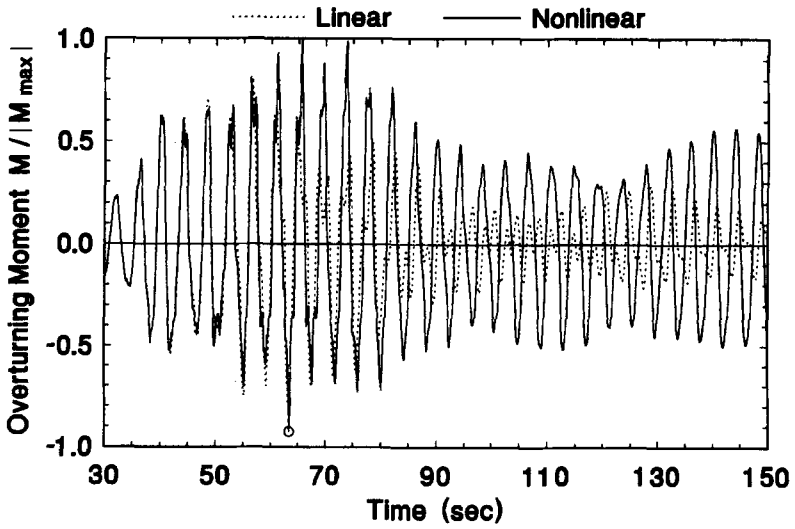


Figure 12. Linear and non-linear overturning moment due to Mexico City SCT1 record ($a$ = 4·57 m (15 ft), $H = a/2$)

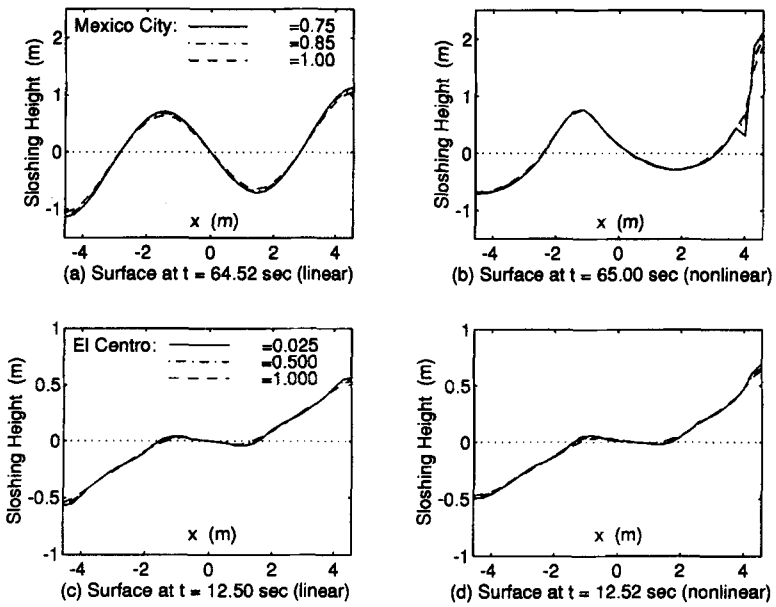


Figure 13. Effects of numerical dissipation on sloshing amplitude

Table IV. Sensitivity of sloshing amplitude at $x = a$ to $\mu$ value

| Earthquake | Linear peak amp (m) | | | Non-linear peak amp (m) | | |
|---|---|---|---|---|---|---|
| | $\mu = 0{\cdot}750$ | $\mu = 0{\cdot}850$ | $\mu = 1{\cdot}000$ | $\mu = 0{\cdot}750$ | $\mu = 0{\cdot}850$ | $\mu = 1{\cdot}000$ |
| Mexico City | 1·14 | 1·11 | 1·06 | 2·13 | 2·04 | 1·89 |
| | Δ per cent | 2·6 | 4·5 | Δ per cent | 4·2 | 7·4 |
| | $\mu = 0{\cdot}025$ | $\mu = 0{\cdot}500$ | $\mu = 1{\cdot}000$ | $\mu = 0{\cdot}025$ | $\mu = 0{\cdot}500$ | $\mu = 1{\cdot}000$ |
| El Centro | 0·57 | 0·55 | 0·54 | 0·70 | 0·66 | 0·64 |
| | Δ per cent | 3·5 | 1·8 | Δ per cent | 5·7 | 3·0 |

the kinematic condition on the free surface to stabilize the erroneous high-frequency waves caused by large convection. It is found that, by adding numerical dissipation at 30–80 per cent of the full upwinding scheme, stable numerical solutions for seismically induced liquid sloshing are generally attainable with a tolerable reduction in peak wave amplitude. The change of liquid mass due to numerical dissipation and the unsymmetric spatial finite difference schemes on the side boundaries are insignificant for engineering applications. The method proposed herein is flexible in that it can be extended to deformable liquid containers and containers with arbitrary shapes.

Severe sloshing occurs when a liquid is subjected to base-excitation records with predominant long-period components such as the Mexico City record. The non-linear sloshing effects are measured by the amount of upward shifting of the sloshing amplitude and the extent of period elongation. It is concluded that non-linear sloshing effects should be considered in seismic-resistant tank design. It would take into account the true sloshing amplitudes which could be in excess of the linear predictions to avoid the damage on the upper part of the structure incurred by the pounding of the excessive hydrodynamic waves. The linear theory was found to be generally non-conservative in the sloshing amplitude but was reasonably accurate in predicting peak hydrodynamic forces. However, the non-conservativeness of the linear theory in predicting the *secondary* peaks of the hydrodynamic forces ought to be taken into consideration in design in order to avoid the cumulative structural damage caused by the repeated excursions of the hydrodynamic forces over the linear prediction.

ACKNOWLEDGEMENT

This study was supported in part by the National Science Foundation (NSF) and the National Center for Earthquake Engineering Research (NCEER). Any findings, conclusions or recommendations are those of the authors, and do not necessarily reflect the views of NSF or NCEER. The allocation of computer resources and the services provided by the staff of Academic Computing at the University of California, Irvine, are also acknowledged with gratitude.

## APPENDIX

*Notation*

| | |
|---|---|
| $a$ | half base-width of liquid container |
| $A_{\max}$ | amplitude of periodic base excitation |
| $C_n(t)$ | time-varying function |
| $g$ | gravitational acceleration |
| $\ddot{G}_X$ | horizontal component of ground acceleration |
| $h$ | free surface elevation measured from quiescent liquid surface |
| $\lvert h_{\max}\rvert$ | maximum sloshing amplitude |
| $H$ | liquid depth measured from the quiescent liquid surface |
| IMAX | maximum number of nodal point in the $\xi$-direction |
| $(\cdot)_{ij}$ | discretized function value at position $i\Delta\xi$ and $j\Delta\eta$ |
| JMAX | maximum number of nodal point in the $\eta$-direction |
| $J(\mathbf{z})$ | Jacobian of Newton–Raphson method evaluated at $\mathbf{z}$ |
| $(\cdot)^k$ | discretized function value at $k$th time step |
| $M$ | overturning moment on liquid container |
| $\lvert M^{\max}_{\text{linear}}\rvert$ | maximum linear overturning moment |
| $\lvert M^{\max}_{\text{non-linear}}\rvert$ | maximum non-linear overturning moment |
| $p$ | hydrodynamic pressure |
| $Q$ | base shear on liquid container |
| $\mathbf{r}$ | Cartesian position vector |
| $S_{an}$ | value of acceleration response spectrum associated with the $n$th linear natural frequency of liquid |

| | |
|---|---|
| $S_1$ | free surface boundary of the liquid domain |
| $S_2$ | liquid boundaries interfacing with container structure |
| $t$ | temporal co-ordinate |
| $\mathbf{u}$ | relative velocity vector of liquid |
| $x, y$ | components of relative Cartesian co-ordinate system |
| ${}^k\mathbf{z}$ | $k$th iterative value of $\mathbf{z}$ |
| $\alpha_n$ | $n$th linear wave number |
| $\Delta t$ | temporal increment |
| $\Delta x, \Delta y$ | spatial increments in $x$- and $y$-directions, respectively |
| $\zeta_n$ | damping ratio associated with the $n$th linear mode of liquid |
| $\mu$ | coefficient between 0·0 and 1·0 |
| $\nu$ | coefficient of second-order numerical dissipation |
| $\xi, \eta$ | two-dimensional curvilinear co-ordinates |
| $\rho$ | liquid mass density |
| $\phi$ | relative velocity potential function |
| $\Omega$ | physical liquid domain |
| $\Omega'$ | computational liquid domain |
| $\omega_n$ | $n$th linear natural frequency of liquid |
| $\bar{\omega}$ | circular frequency of periodic base excitation |

## REFERENCES


1. M. A. Haroun, 'Dynamic analyses of liquid storage tanks', Earthquake Engineering Research Laboratory, *EERL 80-04*, California Institute of Technology, February 1980.
2. M. A. Haroun and G. W. Housner, 'Dynamic interaction of liquid storage tanks and foundation soil', *Proc. 2nd ASCE/EMD specialty conf. on dynamic response of structures*, Atlanta, GA, January 1981, pp. 346–360.
3. M. A. Haroun and M. A. Tayel, 'Response of tanks to vertical seismic excitations', *Earthquake eng. struct. dyn.* **13**, 583–595 (1985).
4. G. W. Housner, 'Dynamic pressure on accelerated fluid containers', *Bull. seism. soc. Am.* **47**, 15–35, (1957).
5. A. S. Veletsos, 'Seismic effects in flexible liquid storage tanks', *Proc. 5th world conf. earthquake eng., Vol. 1*, Rome, Italy, 1974, pp. 630–639.
6. A. S. Veletsos, 'Seismic response and design of liquid storage tanks', in *Guidelines for the Seismic Design of Oil and Gas Pipelines*, Chapter 7, ASCE, New York, 1984, pp. 255–370.
7. A. S. Veletsos, and Y. Tang, 'Dynamics of vertically excited liquid storage tanks', *J. struct. eng., ASCE* **112**, 1228–1246 (1986).
8. H. Abramson, (ed.), '*The Dynamic Behavior of Liquids in Moving Containers*', *NASA SP-106*, Washington, DC, 1966.
9. R. W. Clough, A. Niwa and D. P. Clough 'Experimental seismic study of cylindrical tanks', *J. struct. div. ASCE*, **105**, 2565–2590, (1978).
10. M. A. Haroun and G. W. Housner, 'Vibration tests of full scale liquid storage tanks', in *Proc. 2nd U.S. national conf. earthquake eng.*, Stanford, CA, 1979, pp. 137–145.
11. T. Okamoto, 'Two-dimensional sloshing analysis by Lagrangian finite element method', *Int. j. numer. methods fluids*, **11**, 453–477 (1990).
12. American Petroleum Institute, 'Welded steel tanks for oil storage', API Standard 650, 7th edn, Washington, D.C., 1980.
13. American Water Works Association, 'AWWA standard for welded steel tanks for water storage', AWWA D-100, Denver, Colorado, 1984.
14. R. E. Hutton, 'An investigation of resonant, nonlinear nonplanar free surface oscillations of a fluid', *NASA TN D-1970*, 1963.
15. T. Nakayama and K. Washizu, 'Nonlinear analysis of liquid motion in a container subjected to forced pitching oscillation', *Int. j. numer. methods eng.*, **15**, 1207–1220 (1980).
16. T. Okamoto and M. Kawahara, 'Two-dimensional analysis by the arbitrary Lagrangian–Eulerian finite element method', *Structural Eng./Earthquake Eng., Proc. Japanese society of civil engineers, (No. 441/I-18), Vol. 8, No. 4*, January 1992, pp. 207s–216s.
17. B. Ramaswamy, M. Kawahara and T. Nakayama, 'Lagrangian finite element method for the analysis of two-dimensional sloshing problems', *Int. j. numer. methods fluids*, **6**, 659–670 (1986).
18. W. Chen, 'Nonlinear liquid sloshing motion in seismically-excited rectangular tanks', *Ph.D. Dissertation*, University of California, Irvine, 1993.
19. J. Lighthill, *An Informal Introduction to Theoretical Fluid Mechanics*, Clarendon Press, Oxford, 1986.
20. J. F. Thompson, Z. U. Warsi and C. W. Mastin, *Numerical Grid Generation*, North-Holland, Amsterdam, 1985.
21. W. Minkowycz *et al.* (eds.), *Handbook of Numerical Heat Transfer*, Wiley, New York, 1988.
22. M. A. Haroun and W. Chen, 'Simulation of seismically induced liquid sloshing in tanks: numerical studies', *J. eng. mech. ASCE* (under review).
23. G. Pinder and W. Gary, *Finite Element Simulation in Surface and Subsurface Hydrology*, Academic Press, New York, 1977.